

3D inversion of QMAGT airborne magnetic gradiometry data for susceptibility and magnetization vector models of the Thompson Nickel Belt in Manitoba, Canada

Michael Jorgensen*, and Michael S. Zhdanov, TechnoImaging and Consortium for Electromagnetic Modeling and Inversion, University of Utah
Brian Parsons, Vale Canada LTD

Summary

Following recent advances in SQUID technology, full tensor magnetic gradiometry (FTMG) is emerging as a practical exploration method. We introduce 3D regularized focusing inversion based on the Gramian regularization and moving sensitivity domain to interpret the FTMG data efficiently. A helicopter-borne QMAGT full tensor magnetic gradiometry (FTMG) survey was conducted over the Thompson Nickel Belt by Dias Airborne contracted by Vale Canada LTD. This project aimed to study the location and structure of the P2 member sulfidic meta sedimentary rocks of the Paleoproterozoic Ospwagan Group hosting the Mystery ultramafic intrusion and the associated Ni sulfide mineralization proximal to the survey area. The observed FTMG and calculated total magnetic intensity (TMI) data were analyzed and inverted separately using the developed 3D inversion methods. The data were inverted for susceptibility and magnetization vector models. This is one of the first papers to present the applied inversion of FTMG data towards a magnetization vector model. We also present a comparison of the inversions using the FTMG data and the calculated TMI data.

Introduction

Magnetic vector data measured from orthogonal fluxgate magnetometers are dominated by the earth's background magnetic field and are thus very sensitive to instrument orientation. However, given the relative instabilities of airborne platforms, cesium vapor magnetometers have been preferred, as they directly measure the total magnetic intensity (TMI) and are insensitive to instrument orientation. At the same time, direct measurements of magnetic tensors are advantageous because magnetic tensor data contain directional sensitivity, which is important for determining the rock magnetization vector and studying remanent magnetization. Recently, full tensor magnetic gradiometers based on superconducting quantum interference devices (SQUIDs) have been developed and are now being commercially deployed for geophysical surveying (e.g., Stolz et al., 2006, 2021; Queitsch et al., 2019).

3D inversion of the full tensor magnetic gradiometry data into the magnetization vector is still a challenging problem. The paper presents the recent advances in the FTMG data inversion based on Gramian constraints and moving sensitivity domain approach. We illustrate the developed methods by the results of the 3D inversion of the helicopter-

bore QMAGT full tensor magnetic gradiometry (FTMG) survey conducted over the Thompson Nickel Belt. The survey was aimed to determine the gross geomorphology of the ultramafic intrusion and the associated Ni sulfide mineralization in the northern Thompson Nickel Belt, which is part of the fifth-largest nickel camp in the world (Lightfoot et al., 2016; Franchuk et al., 2015). Dias Airborne collected a total of about 10,500 line km of QMAGT FTMG data in the Thompson Nickel Belt in northern Manitoba, Canada. This paper focuses on the small area of interest (AOI) covered by roughly 100 line-km (Figure 1). The line spacing is 50 m, with sampling every ~2.5 m. The flight height was about 40 m. Figure 1 also shows the digital terrain model (DTM) and flight lines over the AOI.

Traditional inversions for magnetic susceptibility are only sensitive to induced magnetization and often give an incomplete geological picture (Queitsch et al., 2019; Jorgensen and Zhdanov, 2021). The inversion of magnetic data towards a magnetization vector model can provide a more complete picture of geology and mineralization and provide information about the remanent magnetization. In this paper, we use an approximate technique for determining the remanent magnetization. It is based on a decomposition of the full magnetization vector into the amplitudes of inline and perpendicular components relative to the inducing field. The amplitude of inline magnetization can provide models similar to susceptibility but with sharper resolution. The amplitude of perpendicular magnetization is indicative of remanent magnetization, as paramagnetic and ferromagnetic materials tend to be oriented parallel to the inducing field. Similarly, diamagnetic materials (i.e., salt) tend to be oriented in the opposite direction (Tao et al., 2021); however, remanent magnetization can manifest with vectors pointing away from the inducing field. This behavior is schematically illustrated in Figure 2. We present this novel method of the direct imaging of remanent magnetization, which is advantageous to determining optimal exploration strategies.

This paper also demonstrates the advantages of inversion of the FTMG data over the traditional TMI data for mineral exploration. Total field (TMI) data typically require significant post-processing before inversion, including arbitrary filtering, etc. The FTMG data is inherently high-frequency and require only minimal post-processing before inversion, i.e., leveling, outlier removal, etc. The FTMG data are relatively insensitive to instrument orientation since

3D inversion of QMAGT airborne magnetic gradiometry data for susceptibility and magnetization vector models of the Thompson Nickel Belt in Manitoba, Canada

magnetic gradients arise largely from localized sources and not the Earth's background field or regional trends. However, the depth sensitivity of the FTMG data is more limited, i.e., in this case, determined to be roughly 600 m below the surface. This is contrasted with total field sensitivity, which can reach a few kilometers below the surface.

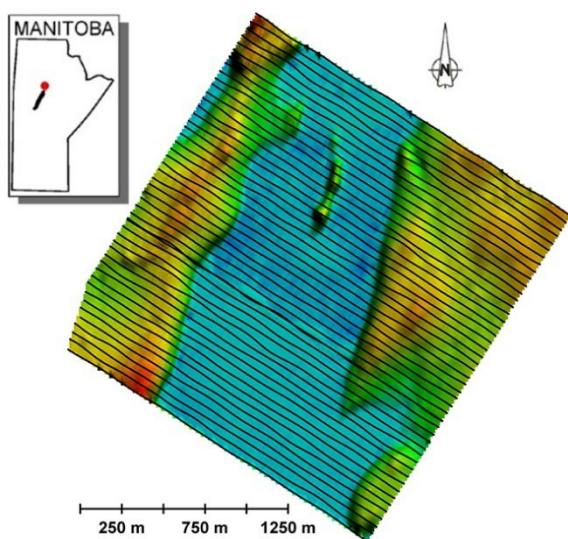


Figure 1: DTM of the QMAGT survey area shown in color. The total relief of the area is 40 m. Survey flight lines are shown by the black lines. The AOI is located in the northern part of the Thompson Nickel Belt in Manitoba, Canada, and is indicated by the red dot in the inset map of Manitoba, shown on the top left side of the figure.

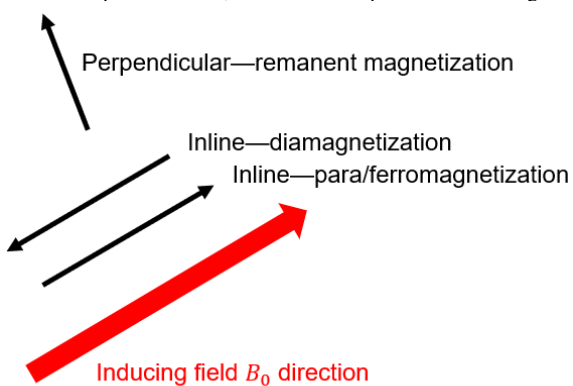


Figure 2: Graphic representation of magnetization vector behavior in different rock types.

Theory

The principles of FTMG data inversion were discussed in several publications (e.g., Zhdanov et al., 2011, 2012; Cuma

et al., 2012, 2014; Queitsch et al., 2019). Therefore, we present a short summary of the developed inversion method here.

The second spatial derivatives of the magnetic potential,

$$B_{\alpha\beta} = \frac{\partial^2}{\partial \alpha \partial \beta} U(\mathbf{r}), \quad \alpha, \beta = x, y, z,$$

form a symmetric magnetic gradient tensor:

$$\hat{\mathbf{B}} = \begin{bmatrix} B_{xx} & B_{xy} & B_{xz} \\ B_{yx} & B_{yy} & B_{yz} \\ B_{zx} & B_{zy} & B_{zz} \end{bmatrix}.$$

The components of magnetization vector, \mathbf{M} , are related to the observed data by linear operator equation

$$\mathbf{d} = \mathbf{A}\mathbf{m}, \quad (1)$$

where \mathbf{d} is a vector of magnetic tensor data; \mathbf{A} is the matrix of the linear operator; and \mathbf{m} is a vector of model parameters, i.e., scalar components of the magnetization vector, \mathbf{M} , on some discretization grid in the inversion domain. By inverting for magnetization vector, one considers the effects of self-demagnetization, anisotropy, and remanent magnetization. The solution of the inverse problem (1) is reduced to minimization of the corresponding parametric functional using the focusing stabilizers and weighting functions. The minimization problem is solved by the re-weighted regularized conjugate gradient (RRCG) method (Zhdanov, 2002, 2015). In order to ensure a robust solution for the magnetization vector, we include an additional Gramian term in the parametric functional. This term enforces the correlation between the different components of the magnetization vector. Details of the magnetization vector inversion algorithm based on Gramian constraints can be found in Jorgensen and Zhdanov (2021).

Finally, the regularized inversion outlined above can be applied to very large-scale problems by incorporating the concept of the moving sensitivity domain (Cox and Zhdanov, 2007; Cuma and Zhdanov, 2014). According to this concept, the sensitivity matrix for the entire large-scale model could be constructed via the superposition of sensitivity domains for all observation points. The sensitivities are also computed "on the fly" during the computations without storing them in the computer memory. This approach makes it possible to invert the data collected by surveys of several thousand line-km on a modest PC cluster as one inversion run.

Susceptibility and magnetization vector models produced by inversion of FTMG data

We have performed independent inversions of the FTMG data for susceptibility and magnetization vector models. All inversions employed a 20 x 40 m horizontal grid with 48 vertical layers ranging from 10-95 m. This accounted for a 2 km inversion domain depth; however, after sensitivity analysis, the models were trimmed to 600 m depth.

3D inversion of QMAGT airborne magnetic gradiometry data for susceptibility and magnetization vector models of the Thompson Nickel Belt in Manitoba, Canada

Tikhonov regularization with minimum support stabilizer was applied to produce the focused images of the magnetized structures (Portniaguine and Zhdanov, 1999; Zhdanov, 2002, 2015, 2018). Figure 3 shows the observed and predicted data for selected FTMG components obtained in the inversion for magnetization vector. The total L2 norm misfit between the observed and predicted data for all six components of the magnetic tensor was reasonably low (under 10%).

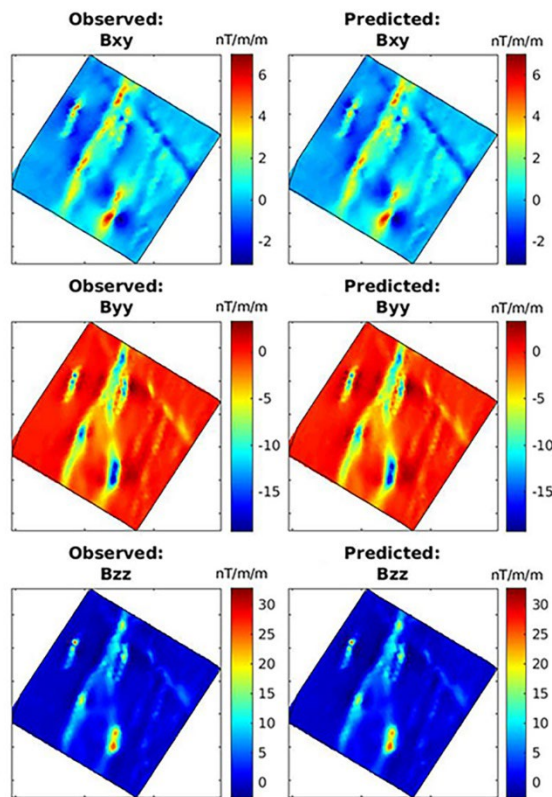


Figure 3: The maps of selected components of the observed and predicted FTMG data from the magnetization vector inversion. All components had a similar level of data misfit.

The inversion parameters for the magnetization vector model are the triaxial X, Y, Z components. We present the inverse models in the form of three characteristics of the full magnetization vector: amplitude, inline amplitude (dia/para/ferromagnetism), and perpendicular amplitude (remanent magnetization). We also plot the projections of the full magnetization vector as black arrows over the color amplitude map.

Figure 4 shows the S-N profiles of the inverted susceptibility and magnetization vector models. In this case, the ultramafic intrusion is apparent as high values (warm colors) in the

susceptibility and inline magnetization models. Conversely, in the remanent magnetization model, the intrusion appears in the low values (cool colors), and the country rocks are imaged in high values. By directly imaging the lithologies near the intrusion, one can better pinpoint potential mineralization targets.

Figure 5 shows the W-E profiles of the magnetic models. The susceptibility model resolves a near-surface anomaly with high susceptibility; however, one can see significantly more structure in the magnetization vector models. In particular, there is a subvertical feature several hundred meters deep directly west of the susceptibility anomaly.

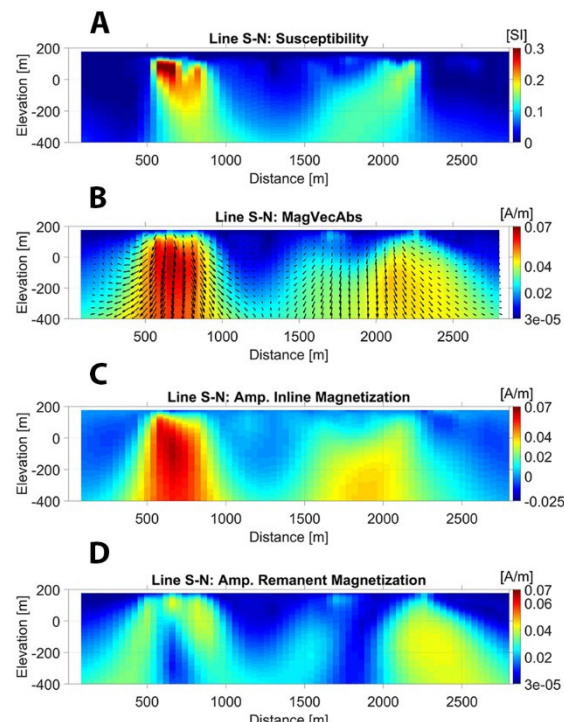


Figure 4: Line S-N profiles of the inverted magnetic models. Panel A shows the magnetic susceptibility model. Panel B shows the amplitude of the magnetization vector in color with the projection of the full magnetization vector shown by the black arrows. Panels C and D show the inline and remanent components of the magnetization vector, respectively.

Comparison of the inversion results using FMTG and TMI data

Figures 6-8 compare the S-N profiles of the susceptibility, inline, and remanent magnetization models, respectively, inverted using the FTMG data and the TMI data which were computed using the tensor data. The advantages of using the FTMG data are clear. The improvement in resolution is

3D inversion of QMAGT airborne magnetic gradiometry data for susceptibility and magnetization vector models of the Thompson Nickel Belt in Manitoba, Canada

comparable to that of airborne gravity gradiometry (AGG) over the vertical gravity total field.

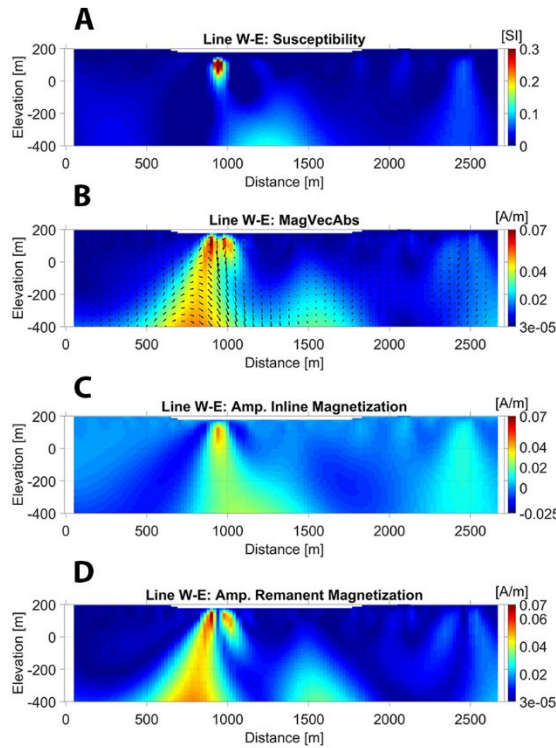


Figure 5: Line W-E profiles of the inverted magnetic models. Panel A shows the magnetic susceptibility model. Panel B shows the amplitude of magnetization vector in color with the projection of the full magnetization vector shown by the black arrows. Panels C and D show the inline component and remanent component of magnetization vector, respectively.

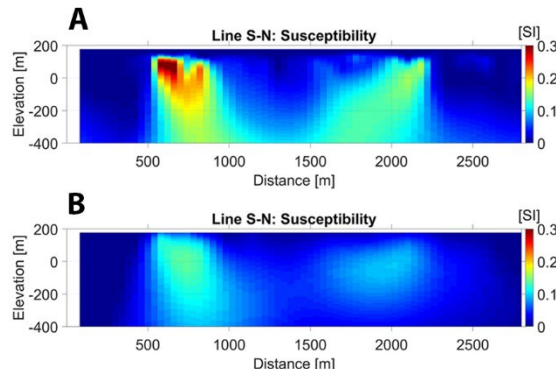


Figure 6: Comparison of the susceptibility models inverted using the FTMG data (Panel A) and the computed TMI data (Panel B).

Conclusions

We have developed and applied a regularized inversion scheme employing a focusing stabilizer and Gramian

constraints to invert FTMG data gathered in the Thompson Nickel Belt.

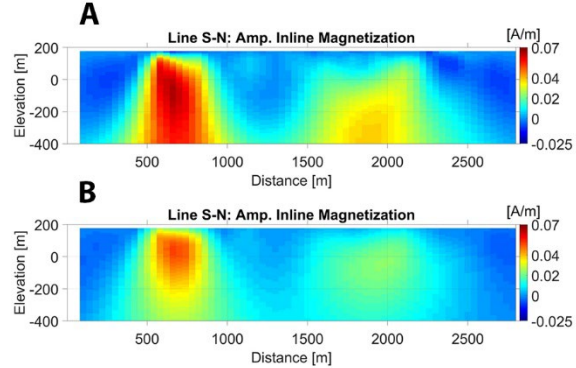


Figure 7: Comparison of the inline magnetization models inverted using the FTMG data (Panel A) and the computed TMI data (Panel B).

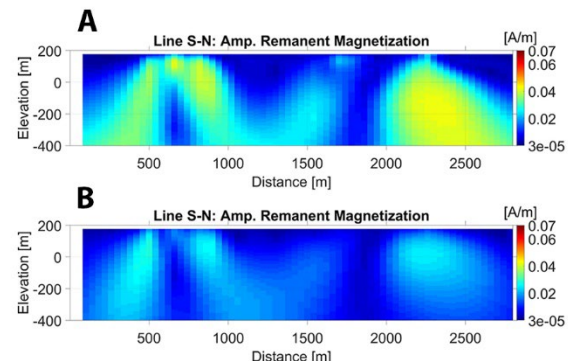


Figure 8: Comparison of the remanent magnetization models inverted using the FTMG data (Panel A) and the computed TMI data (Panel B).

The large ultramafic formation in the area is clearly imaged. Moreover, the surrounding lithologies are also directly imaged in the remanent magnetization transform of the full magnetization vector. The direct imaging of remanent magnetized materials gives a more complete picture of the geology and mineralization of the survey area. We have demonstrated the advantages of the inversion of FTMG data over the traditional TMI data and the advantages of imaging different components of the magnetization vector.

Acknowledgments

The authors acknowledge TechnoImaging and the Consortium for Electromagnetic Modeling and Inversion (CEMI) at The University of Utah for the support of this research project and Dias Airborne and Vale for providing good quality data and permission to publish.

REFERENCES

- Cox, L. H., and M. S. Zhdanov, 2007, Large-scale 3D inversion of HEM data using a moving footprint: 77th Annual International Meeting, SEG, Expanded Abstracts, 467–471.
- Cuma, M., G. A. Wilson, and M. S. Zhdanov, 2012, Large-scale 3D inversion of potential field data: *Geophysical Prospecting*, **60**, 1186–1199.
- Cuma, M., and M. S. Zhdanov, 2014, Massively parallel regularized 3D inversion of potential fields on CPUs and GPUs: *Computers and Geosciences*, **62**, 80–87.
- Franchuk, A., P. C. Lightfoot, and D. J. Kontak, 2015, High tenor Ni-PGE sulfide mineralization in the South Manasian ultramafic intrusion, Paleoproterozoic Thompson Nickel Belt, Manitoba, Canada: *Ore Geology Reviews*, **72**, 434–458, doi: <https://doi.org/10.1016/j.oregeorev.2015.07.021>.
- Jorgensen, M., and M. S. Zhdanov, 2021, Recovering magnetization of rock formations by jointly inverting airborne gravity gradiometry and total magnetic intensity data: *Minerals*, **11**, 366, doi: <https://doi.org/10.3390/min11040366>.
- Lightfoot, P. C., R. Stewart, G. Gribbin, and S. J. Mooney, 2016, Relative contribution of magmatic and post-magmatic processes in the genesis of the Thompson Mine Ni-Co sulfide ores, Manitoba, Canada: *Ore Geology Reviews*, **83**, 258–286, doi: <https://doi.org/10.1016/j.oregeorev.2016.12.017>.
- Portniaguine, O., and M. S. Zhdanov, 1999, Focusing geophysical inversion images: *Geophysics*, **64**, 874–887, doi: <https://doi.org/10.1190/1.1444596>.
- Queitsch, M., M. Schiffler, R. Stolz, C. Rolf, M. Meyer, and N. Kukowski, 2019, Investigation of three-dimensional magnetization of a dolerite intrusion using airborne full tensor magnetic gradiometry (FTMG) data: *Geophysical Journal International*, **217**, 1643–1655.
- Stolz, R., M. Schiffler, V. Zakosarenko, H. Larnier, J. Rudd, G. Chubak, L. Polomé, B. Pitts, M. Schneider, M. Schulz, M. Meyer, and K. Campbell, 2021, Status and future perspectives of airborne magnetic gradiometry: First International Meeting for Applied Geoscience & Energy, SEG/AAPG, Expanded Abstracts, 3554–3561.
- Stolz, R., V. Zakosarenko, M. Schulz, A. Chwala, L. Fritzsch, H. G. Meyer, and E. O. Kostlin, 2006, Magnetic full-tensor SQUID gradiometer system for geophysical applications: *The Leading Edge*, **25**, 178–180, doi: <https://doi.org/10.1190/1.2172308>.
- Tao, M., M. Jorgensen, and M. S. Zhdanov, 2021, Mapping the salt structures from magnetic and gravity gradiometry data in Nordkapp Basin, Barents Sea: First International Meeting for Applied Geoscience & Energy, SEG/AAPG, Expanded Abstracts, Denver.
- Zhdanov, M. S., 2015, Inverse theory and applications in geophysics: Elsevier.
- Zhdanov, M. S., 2018, Foundations of geophysical electromagnetic theory and methods: Elsevier.
- Zhdanov, M. S., H. Cai, and G. A. Wilson, 2011, 3D inversion of full tensor magnetic gradiometry (FTMG) data: 81st Annual International Meeting, SEG, Expanded Abstracts, 791–795.
- Zhdanov, M. S., H. Cai, and G. A. Wilson, 2012, 3D inversion of SQUID magnetic tensor data: *Journal of Geology and Geosciences*, **1**, 1000104, doi: <https://doi.org/10.4172/2329-6755.1000104>.